International Journal of Heat and Mass Transfer 155 (2020) 119645

Contents lists available at ScienceDirect

International Journal of Heat and Mass Transfer

journal homepage: www.elsevier.com/locate/hmt

Surface temperature of a multi-layer thermal barrier coated wall subject to an unsteady heat flux

G. Koutsakis*, G.F. Nellis, J.B. Ghandhi

Engine Research Center, University of Wisconsin-Madison, Madison, WI, 53706, United States

ARTICLE INFO

Article history:
Received 27 December 2019
Revised 6 March 2020
Accepted 11 March 2020
Available online 23 May 2020

Keywords:
Internal combustion engine
Thermal barrier coating
Temperature swing coating
Combustion heat transfer
Low heat rejection engine

ABSTRACT

A one-dimensional analytical method of determining the surface temperature of a thermal barrier coated plane wall subjected to an arbitrarily time-varying heat flux was developed. The method allows fast computation, enabling it to be embedded in combustion simulation software to correctly calculate wall heat transfer, which is important for reciprocating engine applications with thin, low thermal inertia coatings that have large temperature swings. The method relies on superposition of the response to successive step changes in heat flux, obtained by discretizing the heat flux history, to compile the solution. The embedded problem of a step-change in heat flux is addressed using the one-dimensional heat diffusion equation in conjunction with the matrix method in the Laplace domain, assuming the lateral conduction is neglected. For a two-layer wall (one coating layer on top of the metal wall) in the limit where $\sqrt{k\rho c}$ of the coating is small relative to that for the wall material, an analytical inversion to the time domain can be derived. For modest values of this parameter or for more than one coating layer, the residue theorem is invoked to invert to the time domain, with the poles and residues found numerically. The analytical inversion, however, provided the impetus for defining a set of non-dimensional parameters that uniquely characterize the surface temperature swing for arbitrary periodic heat flux to the wall. Non-dimensional results are given for a sinusoidally varying surface heat flux.

1. Introduction

The performance of an internal combustion engine depends upon the successful extraction of work from the chemical energy supplied. A fraction of the chemical energy release is lost to the coolant as heat through the combustion chamber surface, and from there it is rejected to the ambient. Depending on operating condition, 20–40% of the fuel energy is lost to the coolant [1]. The reduction of this heat loss could potentially improve the fuel economy, *i.e.*, the engine's thermal efficiency, and reduce the cooling system requirements. Applying thermal barrier coatings (TBC) to in-cylinder surfaces is one route toward decreasing heat loss.

During the late 1970s, attempts were initiated within the internal combustion engine research community to develop the so called adiabatic engine [2,3]. Early experimental investigations were conducted using thermal barrier coating materials adapted from gas turbine applications [4]. The TBC were deposited on the power cylinder component surfaces, *e.g.* the piston crown, cylinder head, intake/exhaust valves, cylinder liner and exhaust ports. A typical TBC consisted of four layers: the substrate or metal engine wall made out of steel or aluminum alloys; the bond-coat typically made of NiCrAlY alloy; a thermally grown oxide; and the ceramic top-coat. The latter was typically yttria stabilized zirconia (YSZ) or silicon nitride (Si_3N_4). In comparison to the base metal wall, the effective coating properties (including contact resistances and bond coat) had lower thermal conductivity (~1 *vs.* ~100 W/(mK)) and almost equivalent volumetric heat capacity (~2.5 MJ/(m^3K) *vs.* ~3.0 MJ/(m^3K)).

Surface heat fluxes to reciprocating-engine combustion chamber surfaces are unsteady and non-uniform in space. Close to the combustion event in a heavy-duty diesel engine at high load, the peak heat flux can reach 10 MW/m^2 [5]. Engine cycle time scales usually vary from 20-200ms. During the intake stroke, heat often flows from the hot combustion chamber surfaces to the fresh charge; this heating leads to a decrease in volumetric efficiency, *i.e.*, how much air can be inducted, which limits power output. The exhaust gas exits past the exhaust valves, and through the ports, manifolds, turbochargers and after-treatment devices, all of which play an important role in the overall system thermal management. By insulating the chamber walls with coatings, one would intuitively think that the result would be an increase in the shaft work.

The performance of these initial coating formulations, however, has been mixed. Several authors have reported a reduction in fuel

* Corresponding author.
E-mail address: koutsakis@wisc.edu (G. Koutsakis).

https://doi.org/10.1016/j.ijheatmasstransfer.2020.119645
0017-9310/

Nomenclature

$\dot{q}''$	Surface Heat Flux [Wm^{-2}]
$\bar{q}''$	Mean Surface Heat Flux [Wm^{-2}]
h	Heat transfer coefficient [$Wm^{-2}K^{-1}$]
t	Temperature [K]
Θ	Dimensionless Temperature [-]
θ	Time [s]
α	Thermal diffusivity [m^2s^{-1}]
k	Thermal conductivity [$Wm^{-1}K^{-1}$]
ρ	Density [kgm^{-3}]
c	Specific heat capacity [$Jkg^{-1}K^{-1}$]
ρ **c**	Volumetric heat capacity [$Jm^{-3}K^{-1}$]
x	Distance [m]
L	Length [m]
A,B,C,D	Matrix coefficients
R	Thermal resistance [m^2KW^{-1}]
C	Capacitance per unit area [$Jm^{-2}K^{-1}$]
s	Laplace, frequency variable [Hz]
β	Positive real number and simple root of D(s) [Hz]
Λ	Thermal inertia ratio [-]
ν	Summation term [-]
f	Excitation frequency [Hz]
Ξ	Dimensionless thermal resistance ratio [-]
Ω_1	Dimensionless coating time scale [-]
Ω_2	Dimensionless wall time scale [-]

Subscripts

g	gas
w	wall
c	coolant
m	root index

Abbreviations

TBC	Thermal Barrier Coating
YSZ	Yttria Stabilized Zirconia
TS	Thermal-swing
SiRPA	Silica-Reinforced Porous Anodized Aluminum
HVLP	High Volume Low Pressure

consumption with TBC engine components [6–9], but other authors have reported comparable of worse fuel consumption [9–13]. Some of this discrepancy can be attributed to the fact that optimal performance with coated components is not necessarily achieved at the same operating conditions as in the uncoated engine, and not all studies take the effort to compare best-case performance results. There is a similar disagreement about whether the higher wall temperature affects the fundamental heat transfer process. Some researchers suggest that the heat transfer coefficient is increased with the higher wall temperature [14–16], while others suggest that the heat transfer coefficient is largely unchanged by the elevated wall temperature [6,13,17,18].

The concept of a temperature-swing coating was recently introduced [19] for reciprocating engine combustion chamber heat insulation. The proposed coatings have slightly lower thermal conductivity and significantly lower volumetric heat capacity than earlier generation coatings; this is achieved by deliberately encouraging high porosity. With such properties, the wall surface temperature tends to follow the gas temperature more closely during the cycle, and the resulting reduction in temperature difference reduces wall heat transfer over the entire engine cycle. Toyota developed the SiRPA coating by anodizing the piston surface, reinforcing the pores with silica and sealing the surface [20]. The successful implementation of the SiRPA coating was demonstrated [21] and resulted in lower fuel consumption and higher cold-start efficiency despite insulating just the squish area of the piston. Durrett *et al.* [22] have developed a similar coating made of sintered hollow nickel-alloy micro-spheres to effect higher porosity. Andrie *et al.* demonstrated reliable spark-ignited engine operation [23] using a high volume low pressure (HVLP) method; two coatings with outstanding coating properties were developed. This new generation of temperature-swing coatings typically have thermal conductivity about one quarter that of zirconia and volumetric heat capacity around one third that of zirconia.

Prediction of the surface temperature of a TBC combustion chamber has been calculated by assuming one-dimensional heat flow in the wall and applying a finite difference solution. The relatively thin coatings and short time scales, however, require fine grid resolution and small time steps to ensure stability and accuracy (particularly near the surface) [24,25]. Some earlier studies used thermal network models [26–30], but these can effectively be considered very low-fidelity finite difference methods. The successful application of TBC requires optimization of the entire engine system, including the full exhaust system, which can only be readily achieved using complex, commercially available codes. Coupling a 1-D finite difference wall conduction model to such a code makes these calculations extremely time consuming and less useful for design.

The objective of this work is to develop a one-dimensional analytical methodology to accurately predict the surface temperature of a multi-layer thermal barrier coated plane wall. The resulting time-varying wall temperature can be using in conjunction with a zero-dimensional combustion simulation that computes the gas temperature and heat transfer coefficient to determine the overall wall heat transfer rate. It should be noted that for 0-D engine combustion simulations a global heat transfer coefficient is used that accounts for the spatially non-uniform heat flux. Thus the assumption of 1-D conclusion in the wall is justified [31]. The method relies only on heat flux history to derive the time-resolved wall temperature. The analytical nature of the solution enables fast computation to allow system-level optimization calculations.

2. Mathematical model

2.1. Model setup

Consider thermal diffusion in a solid 1-D multi-layer (any number of layers is allowable) plane wall with overall thickness L and constant thermophysical properties within each layer, as shown in Fig. 1. The governing heat diffusion equation is

$$k\frac{\partial^2 t}{\partial x^2} = \rho c\frac{\partial t}{\partial \theta} \tag{1}$$

where t is temperature, θ is time, k and ρc are thermal conductivity and volumetric heat capacity, respectively. The $x = 0$ location represents the combustion chamber surface where a time-varying heat flux, $\dot{q}''(\theta)$, is imposed

$$-k\frac{\partial t}{\partial x}\bigg|_{x=0} = \dot{q}''(\theta) = f(\theta) \tag{2}$$

A heat flux boundary condition is used instead of a convective boundary because both the gas temperature and heat transfer coefficient change with time in an engine.

The applied heat flux is periodic in a reciprocating engine and one is often interested in the converged periodic solution. For this case, the temperature at $x = L$ is constant and, for simplicity, equal to the coolant temperature, t_c,

$$t_{x=L,\theta\to\infty} = t_c \tag{3}$$

and the wall temperature distribution oscillates about a steady-state distribution, which is found trivially from the mean (over the

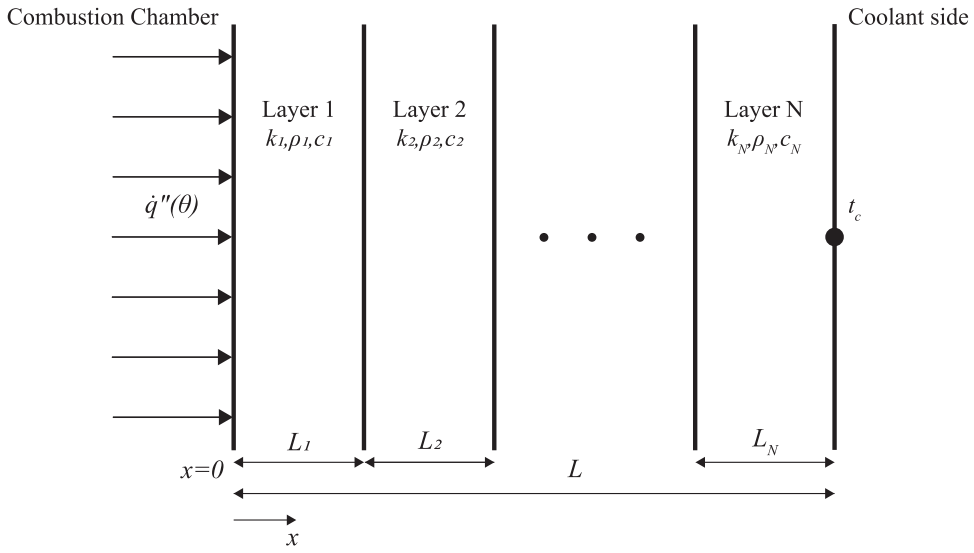

Fig. 1. Illustration of an 1-D multi-layer engine wall. The boundary condition on the combustion chamber gas-side is assumed to be a time dependent heat flux, while the coolant side experiences a constant temperature.

cycle) surface heat flux, $\bar{q}''$ and the backside temperature in (3). In practice, in order to more rapidly reach the converged periodic condition, the steady-state temperature distribution is used as an initial state as will be discussed below.

The unsteady part of this problem, which will be dealt with in subsequent sections, has an initial wall temperature that is uniform and taken as zero.

$$t_{\theta=0} = 0 \tag{4}$$

In this formulation, the problem relies only on the prescribed heat flux, including data from the past to solve for the gas-side wall surface temperature. The time-dependent wall temperature can then be used in the gas-side convective cooling model, as compared to assuming a constant wall temperature, to more accurately predict heat flow to the wall.

2.2. Superposition

For the proposed problem with constant layer thermophysical properties, the governing partial differential equation is linear and homogeneous. Thus, the solution can be found using the principle of superposition. The surface temperature of a wall subjected to $\dot{q}''(\theta)$ can be found as the summation of the responses to a series of step changes in surface heat flux taking place at successive times. Fig. 2 illustrates this concept for an arbitrary applied heat flux. For example, the temperature at θ_5 is found by first discretizing the heat flux into a sequence of step changes in heat flux (see Fig. 2). The surface temperature response to each heat flux step is found from the solution of the heat diffusion equation. The surface temperature is then the sum of the step responses before θ_5, then at θ_5: $t_{x=0}(\theta_5) = t_{o,1}(\theta_5 - \theta_1) + t_{o,2}(\theta_5 - \theta_2) + \ldots + t_{o,4}(\theta_5 - \theta_4)$.

2.2.1. Initial condition

By posing the problem with the boundary conditions (2) and (4) there will be a very long starting transient, that is it will take a large number of cycles to reach the periodic converged solution. For example, the imposition of a step change of heat flux $\bar{q}''$ to the surface will result (for a homogeneous wall) in an increase of surface temperature with a square root dependence on time [24]. This issue can be mitigated using the superposition framework. One can envision that for $\theta < 0$, there is a steady heat flux $\bar{q}''$ into the wall that establishes a steady, piece-wise linear temperature distribution. At time $\theta = 0$, the steady state heat flux will turn off, and it is replaced by the successive incremental step changes as discussed above. The net effect is the same as solving the problem with the initial temperature distribution of a steady state case.

3. Step-change solution

The solution to the coated wall problem subject to a step change in heat flux can be found using the methodology established initially by Pipes [32] and later by Carslaw and Jaeger [33] based on taking the Laplace transform of Eq. (1). Using the notation $\hat{t}$ is the Laplace transform of surface temperature, and likewise $\hat{q}$ is the transform of surface heat flux, one can write for layer 1 the transformed general solution of the differential equation as

$$\hat{t}(x,s) = A\cosh\left(x\sqrt{\frac{s}{\alpha}}\right) + B\sinh\left(x\sqrt{\frac{s}{\alpha}}\right) \tag{5}$$

where K_1, K_2 are constants and α is thermal diffusivity. By differentiating Eq. (5) the general form of the heat flux becomes

$$\hat{q}(x,s) = -kK_1\sqrt{\frac{s}{\alpha}}\sinh\left(x\sqrt{\frac{s}{\alpha}}\right) - kK_2\sqrt{\frac{s}{\alpha}}\cosh\left(x\sqrt{\frac{s}{\alpha}}\right) \tag{6}$$

By evaluating $\hat{t}$ and $\hat{q}$ at $x = 0$ and $x = L_1$, and rearranging to eliminate constants K_1 and K_2 one gets

$$\hat{t}(0,s) = \underbrace{\left[\cosh\left(L_1\sqrt{\frac{s}{\alpha}}\right)\right]}_{A_1(s)}\hat{t}(L_1,s) + \underbrace{\left[\frac{\sinh\left(L_1\sqrt{\frac{s}{\alpha}}\right)}{k\sqrt{\frac{s}{\alpha}}}\right]}_{B_1(s)}\hat{q}(L_1,s) \tag{7}$$

$$\hat{q}(0,s) = \underbrace{\left[k\sqrt{\frac{s}{\alpha}}\sinh\left(L_1\sqrt{\frac{s}{\alpha}}\right)\right]}_{C_1(s)}\hat{t}(L_1,s) + \underbrace{\left[\cosh\left(L_1\sqrt{\frac{s}{\alpha}}\right)\right]}_{D_1(s)}\hat{q}(L_1,s) \tag{8}$$

Using the notation $\hat{t}_o(s) = \hat{t}(0,s)$ and $\hat{t}_1(s) = \hat{t}(L,s)$, and similarly for $\hat{q}$ one finds

$$\hat{t}_o(s) = A_1(s)\cdot\hat{t}_1(s) + B_1(s)\cdot\hat{q}_1(s) \tag{9}$$

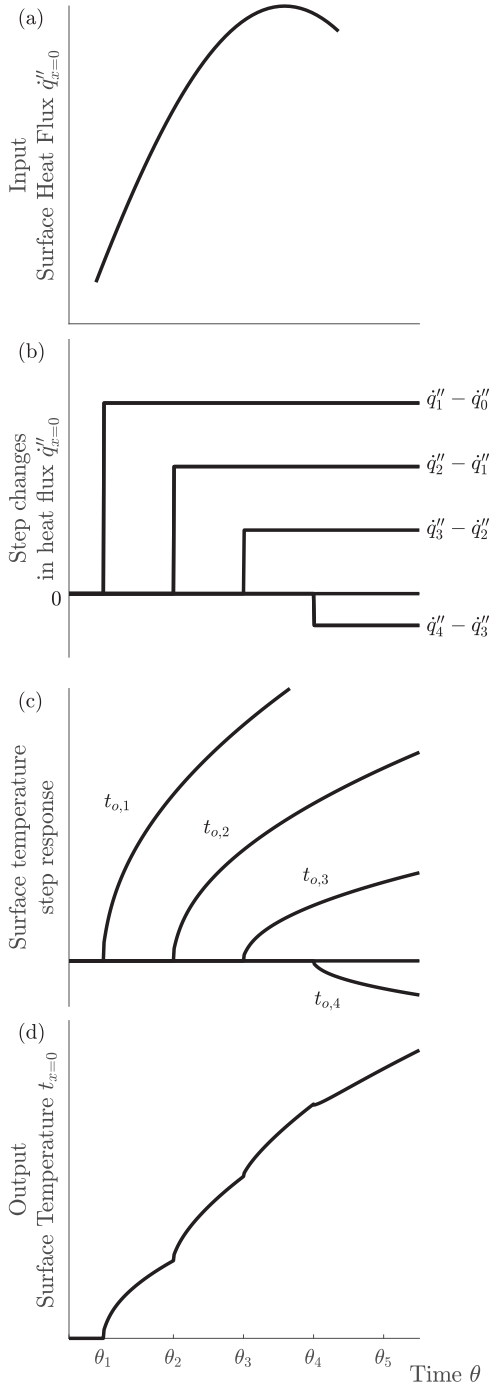

Fig. 2. (a) Input continuous surface heat flux as a function of time approximated by (b) a series of step changes. (c) Output individual surface temperature step responses and (d) Total surface temperature is the sum of these step responses.

$$t_o(\theta) = \mathbf{1} \cdot \mathcal{L}^{-1}\left\{ \frac{1}{s} \frac{\frac{R_1}{\sqrt{sR_1C_1}} \sinh\sqrt{sR_1C_1}\cosh\sqrt{sR_2C_2} + \frac{R_2}{\sqrt{sR_2C_2}} \cosh\sqrt{sR_1C_1}\sinh\sqrt{sR_2C_2}}{\Lambda \sinh\sqrt{sR_1C_1}\sinh\sqrt{sR_2C_2} + \cosh\sqrt{sR_1C_1}\cosh\sqrt{sR_2C_2}} \right\} \tag{17}$$

$$\hat{q}_o(s) = C_1(s)\cdot\hat{t}_1(s) + D_1(s)\cdot\hat{q}_1(s) \tag{10}$$

or in matrix form:

$$\begin{bmatrix}\hat{t}_o \\ \hat{q}_o\end{bmatrix} = \begin{bmatrix}A_1(s) & B_1(s) \\ C_1(s) & D_1(s)\end{bmatrix}\begin{bmatrix}\hat{t}_1 \\ \hat{q}_1\end{bmatrix} \tag{11}$$

The coefficients of the matrix in (11) can be written as

$$\begin{bmatrix}A_1(s) & B_1(s) \\ C_1(s) & D_1(s)\end{bmatrix} = \begin{bmatrix}\cosh\sqrt{sR_1C_1} & \frac{R_1}{\sqrt{sR_1C_1}}\sinh\sqrt{sR_1C_1} \\ \frac{\sqrt{sR_1C_1}}{R_1}\sinh\sqrt{sR_1C_1} & \cosh\sqrt{sR_1C_1}\end{bmatrix} \tag{12}$$

where $R_1 = \frac{L_1}{k_1}$ is the thermal resistance per unit area and $C_1 = L_1\rho_1 c_1$ is the volumetric heat capacity per unit area. The above relation (11) may also be written in the following form to take advantage of the known boundary conditions $\hat{t}_1$ (ultimately at $x = L$) and $\hat{q}_o$

$$\begin{bmatrix}\hat{t}_o \\ \hat{q}_1\end{bmatrix} = \begin{bmatrix}\frac{AD-BC}{D} & \frac{B}{D} \\ -\frac{C}{D} & \frac{1}{D}\end{bmatrix}\begin{bmatrix}\hat{t}_1 \\ \hat{q}_o\end{bmatrix} \tag{13}$$

The first element of the transfer matrix can be simplified to

$$A_1D_1 - B_1C_1 = \cosh^2\sqrt{sR_1C_1} - \sinh^2\sqrt{sR_1C_1} = 1 \tag{14}$$

and in general $A_iD_i - B_iC_i = 1$ is the determinant of the matrix (12) for $i = 1..N$ layers. This approach can be extended to any number of layers

$$\begin{bmatrix}A(s) & B(s) \\ C(s) & D(s)\end{bmatrix} = \begin{bmatrix}A_1(s) & B_1(s) \\ C_1(s) & D_1(s)\end{bmatrix}\cdot\begin{bmatrix}A_2(s) & B_2(s) \\ C_2(s) & D_2(s)\end{bmatrix}\cdots \begin{bmatrix}A_N(s) & B_N(s) \\ C_N(s) & D_N(s)\end{bmatrix} \tag{15}$$

3.1. Methodology

The two-layer problem, which has been the physical model employed in the past for a coated wall, will be used to demonstrate the solution methodology. Later it will be extended to any number of layers. For a two-layer problem having a relatively thin coating and the metal wall as the second layer, the analogous form of Eq. (13) using the overall transfer matrix is

$$\begin{bmatrix}\hat{t}_o \\ \hat{q}_2\end{bmatrix} = \begin{bmatrix}\frac{1}{C_1B_2 + D_1D_2} & \frac{A_1B_2 + B_1D_2}{C_1B_2 + D_1D_2} \\ -\frac{C_1A_2 + D_1C_2}{C_1B_2 + D_1D_2} & \frac{1}{C_1B_2 + D_1D_2}\end{bmatrix}\begin{bmatrix}\hat{t}_2 \\ \hat{q}_0\end{bmatrix} \tag{16}$$

From matrix algebra the *transform* of surface temperature, $\hat{t}_0$, can be determined using Eq. (16). From Eq. (4), $\hat{t}_2 = 0$ and the Laplace transform of the Heaviside function of unity magnitude, *i.e.*, $\hat{q}_o$ (the magnitude of the heat flux step will be added later) is $\frac{1}{s}$. The surface temperature in the time domain is then found from the *inverse transform* of $\hat{t}_0$, which can be written as

where $\Lambda = \sqrt{\frac{R_2C_1}{R_1C_2}} = \sqrt{\frac{k_1\rho_1c_1}{k_2\rho_2c_2}}$ is the ratio of thermal inertia of the coating to the thermal inertia of the metal wall.

The inverse Laplace transform for the equation above is not readily available in transform tables. Problems of this kind can be approached in two different ways. The first is by applying multiple geometric series expansions to bring the transform into a form that is included in Laplace transform tables. This approach requires significant algebra and the result does not necessarily lend itself to

engineering applications [33]. The second approach is to utilize the general formula of the inverse Laplace transform

$$t_o(\theta) = \mathbf{1} \cdot \frac{1}{2\pi j} \int_{\Omega - j\infty}^{\Omega + j\infty} \hat{t}(s) e^{s\theta} ds \tag{18}$$

where $j = \sqrt{-1}$ and the constant Ω is a large positive real number approaching infinity. The Cauchy residue theorem states that the above integral is equal $2\pi j$ times the sum of the residues of $\hat{t}(s)$ at the poles of $\hat{t}(s)e^{s\theta}$. Also, it has been shown that the branch cut of $\sqrt{sRC}$ does not include the negative real axis [34].

3.2. Two-layer problem, $\Lambda \to 0$

The use of thin, low thermal conductivity, low-volumetric heat capacity coating materials is of high interest. The thermal inertia of thermal-swing coatings described above are quite low, and the resulting thermal inertia ratio for a typical metal wall is correspondingly small ($\Lambda \simeq 0.015 - 0.025$). This observation allows the assumption of $\Lambda \to 0$ which in turn allows a simplification of Eq. (17) to

$$t_o(\theta) = \mathbf{1} \cdot \left[R_1 \cdot \mathcal{L}^{-1} \left\{ \frac{\sinh\sqrt{sR_1C_1}}{s\sqrt{sR_1C_1}\cosh\sqrt{sR_1C_1}} \right\} + R_2 \cdot \mathcal{L}^{-1} \left\{ \frac{\sinh\sqrt{sR_2C_2}}{s\sqrt{sR_2C_2}\cosh\sqrt{sR_2C_2}} \right\} \right] \tag{19}$$

Consider the function:

$$\Phi_i(s) = \frac{\sinh\sqrt{sR_iC_i}}{s\sqrt{sR_iC_i}\cosh\sqrt{sR_iC_i}} \tag{20}$$

where $i = 1, 2$. The function $\Phi(s)$ has poles at $s_o = 0$, and at $\sqrt{s_\nu R_i C_i} = \frac{2\nu-1}{2}\pi j$ where $\nu = 1, 2 \ldots$. The latter can also be written as $s_\nu = -\frac{(2\nu-1)^2}{4R_iC_i}\pi^2$. The simple pole at $s_o = 0$ for the function $\Phi_i(s)$ gives residue

$$\begin{aligned}
\mathrm{Res}(\Phi_i; s_o) &= \lim_{s\to s_o} \left[s \frac{\sinh\sqrt{sR_iC_i}}{s\sqrt{sR_iC_i}\cosh\sqrt{sR_iC_i}} e^{s\theta} \right] \\
&= \lim_{s\to 0} \left[\frac{\left(\sqrt{sR_iC_i}\right) + \frac{\left(\sqrt{sR_iC_i}\right)^3}{3!} + \ldots}{\sqrt{sR_iC_i}\left[1 + \frac{\left(\sqrt{sR_iC_i}\right)^2}{2!} + \ldots\right]} e^{s\theta} \right] \\
&= \lim_{s\to 0} \left[\frac{1 + \frac{\left(\sqrt{sR_iC_i}\right)^2}{3!} + \cdots}{1 + \frac{\left(\sqrt{sR_iC_i}\right)^2}{2!} + \ldots} e^{s\theta} \right] \\
&= 1
\end{aligned} \tag{21}$$

For the singularities at $s_\nu = -\frac{(2\nu-1)^2}{4R_iC_i}\pi^2$, one can write $\Phi(s) = \frac{f(s)}{g(s)}$, with $f(s) = \sinh\sqrt{sR_iC_i}$ and $g(s) = s\sqrt{sR_iC_i}\cosh\sqrt{sR_iC_i}$. The residue can then be found as [34]

$$\begin{aligned}
\mathrm{Res}(\Phi; s_\nu) &= \frac{f(s_\nu)}{\frac{dg}{ds}|_{s_\nu}} e^{s_\nu\theta} \\
&= \frac{\sinh\sqrt{sR_iC_i}}{\frac{3}{2}\sqrt{sR_iC_i}\cosh\sqrt{sR_iC_i} + \frac{sR_iC_i}{2}\sinh\sqrt{sR_iC_i}} e^{s_\nu\theta} \\
&= \frac{1}{\frac{1}{2}\left[\frac{2\nu-1}{2}\pi j\right]^2} e^{-\frac{(2\nu-1)^2}{4R_iC_i}\pi^2\theta} \\
&= -\frac{8}{\pi^2(2\nu-1)^2} e^{-\frac{(2\nu-1)^2}{4R_iC_i}\pi^2\theta}
\end{aligned} \tag{22}$$

Using the values of the residues predicted by Eq. (22) in Eq. (19), the surface temperature as a function of time for the two-layer problem with negligible thermal inertia ratio subjected to a unit step change of heat flux on the suface is obtained

$$t_o(\theta) = \mathbf{1} \cdot \left[R_1 \left(1 - \frac{8}{\pi^2} \sum_{\nu=1}^{\infty} \frac{1}{(2\nu-1)^2} e^{-\frac{(2\nu-1)^2}{4R_1C_1}\pi^2\theta} \right) + R_2 \left(1 - \frac{8}{\pi^2} \sum_{\nu=1}^{\infty} \frac{1}{(2\nu-1)^2} e^{-\frac{(2\nu-1)^2}{4R_2C_2}\pi^2\theta} \right) \right] \tag{23}$$

3.3. Multi-layer problem

The overall transfer matrix of the multi-layer wall was given by (15) and recasting the problem in the manner that takes advantage of the known boundary conditions, Eq. (13), one gets

$$\begin{bmatrix} \hat{t}_o \\ \hat{q}_N \end{bmatrix} = \begin{bmatrix} \frac{1}{D} & \frac{B}{D} \\ -\frac{C}{D} & \frac{1}{D} \end{bmatrix} \begin{bmatrix} \hat{t}_N \\ \hat{q}_o \end{bmatrix} \tag{24}$$

where, similar to the case of a single layer, the determinant $AD - BC$ is found to be unity. Using the fact that $\hat{t}_N = 0$, the above formula becomes $\hat{t}_o = \frac{B}{D} \cdot \hat{q}_o$. By applying a step impulse of heat flux with unity magnitude such that $\hat{q}_o = \mathbf{1} \cdot \frac{1}{s}$, the corresponding function, Ψ, that needs to be inverse tranformed is

$$\Psi = \frac{1}{s}\frac{B(s)}{D(s)} \tag{25}$$

There is a simple pole at $s_0 = 0$, but finding the roots of $D(s) = 0$ is non-trivial, especially as the number of layers gets large. Carslaw and Jaeger, however, have shown in a two-layer wall problem with different boundary conditions and unknowns that all of the roots lie on the negative real axis and are simple [33]. Therefore, numerical techniques can be employed to find and tabulate the roots unless other simplifying assumptions can be made.

The roots of $D(s) = 0$ can be found as $B(s)|_{s=-\beta_m}$ where $m = 1, 2 \ldots \infty$. Applying the residue theorem

$$\begin{aligned}
\mathcal{L}^{-1}\{\Psi\} &= \mathrm{Res}(\Psi; 0) + \sum_{m=1}^{\infty} \mathrm{Res}(\Psi; -\beta_m) \\
&= \lim_{s\to 0}\left[s\frac{1}{s}\frac{B(s)}{D(s)} e^{s\theta} \right] + \sum_{m=1}^{\infty} \left[\frac{B(s)|_{s=-\beta_m}}{-\beta_m \frac{dD(s)}{ds}|_{s=-\beta_m}} e^{-\beta_m\theta} \right] \\
&= \lim_{s\to 0}\left[\frac{B(s)}{D(s)} e^{s\theta} \right] - \sum_{m=1}^{\infty} \left[\frac{B(s)|_{s=-\beta_m}}{\beta_m \frac{dD(s)}{ds}|_{s=-\beta_m}} e^{-\beta_m\theta} \right] \\
&= \frac{B(0^+)}{D(0^+)} - \sum_{m=1}^{\infty} \left[\frac{B(s)|_{s=-\beta_m}}{\beta_m \frac{dD(s)}{ds}|_{s=-\beta_m}} e^{-\beta_m\theta} \right]
\end{aligned} \tag{26}$$

Additionally, it has been verified that for any number of layers the $\lim_{s\to 0^+} B(s) = B(0^+) = R_{total}$ and $\lim_{s\to 0^+} D(s) = D(0^+) = 1$. Finally, the surface temperature history as a function of time is given by

$$t_o(\theta) = \mathbf{1} \cdot \left[R_{total} - \sum_{m=1}^{\infty} \frac{B(s)|_{s=-\beta_m}}{\beta_m \frac{dD(s)}{ds}|_{s=-\beta_m}} e^{-\beta_m\theta} \right] \tag{27}$$

3.4. Step-change comparison

A 1-D plane wall finite difference code was used to verify the two-layer solution of (27) and to evaluate the limitations of the $\Lambda \to 0$ solution in (23) for a step-change in surface heat flux. At time $\theta = 0$, a 1 MW/m^2 step change of heat flux was imposed at $x = 0$. The finite difference code included 400 nodes in the coating and 601 nodes in the metal substrate, including the interface node.

Table 1
Properties of coating and engine wall materials.

	k $[W/(mK)]$	ρc $[J/(m^3K)]$	L $[\mu m]$	$\sqrt{k\rho c}$ $[J/(m^2Ks^{0.5})]$	Λ [-]	RC $[ms]$
TS	0.35	4.0×10^5	100	0.374	0.015	11.4
YSZ	1.3	2.5×10^6	100	1.803	0.075	19.2
Aluminum	213	2.4×10^6	4900	23.85	-	-

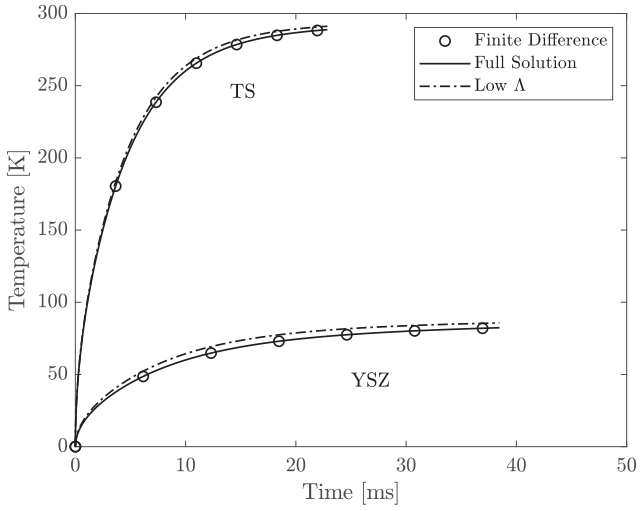

Fig. 3. Transient surface temperature predicted by the approximate two-layer solution (solid) and the finite difference code (dashed) for a uniform initial temperature subjected to 1 MW/m^2 step-change in surface heat flux for TS and YSZ coatings. The complete solution derived by the full inversion is also known.

The simulation was performed for 5000 time-steps up to a time equal to $2R_1C_1$, *i.e.,* twice the coating characteristic time scale.

Two test cases will be illustrated by way of example. The two coating materials shown in Table 1 represent (1) a state-of-the-art thermal-swing (TS) coating, and (2) a traditional 8% YSZ coating [23]; in both cases the base material was aluminum and the total domain length was 5mm. The TS coating was evaluated with a 100 μm thickness that gives a characteristic time scale of 11.4ms. The YSZ coating was evaluated with a 100 μm thickness resulting in a characteristic time scale of 19.2ms. Fig. 3 shows the surface temperature as a function of time for the two coatings. For each case the finite difference, full inversion solution, (27), and the low-Λ limit solution, (23), curves are shown, with the former taken as the reference.

Fig. 3 shows that the full inversion solution, which was calculated using just the first 100 roots, tracks the finite difference solution very closely. The low-Λ solution also shows reasonable agreement for the two cases, albeit with some error. This difference is expected given the finite values of Λ seen in Table 1, and the YSZ coating, which has the larger value of Λ shows worse agreement.

In order to evaluate the limits of the proposed low-Λ approximate solution, the RMS error - using the finite difference code as a reference - was calculated for a wide range of coating properties but fixed substrate properties (of Aluminum, see Table 1). More specifically, for every Λ ranging from 0.01-0.05 the product of $k_1\rho_1c_1$ was held fixed. The time scale of the hypothetical coating was varied from 1 to 100 ms through the coating thickness. Fig. 4 shows that Λ alone does not control the observed error, the coating time scale, R_1C_1 also affects the results. At a given coating time scale, the error increases monotonically with Λ, as expected. However, for a constant value of Λ the error can be seen to decrease as the coating timescale increases. There appears to be a counter-acting effect of R_1C_1 in Eq. (17); a similar effect may also

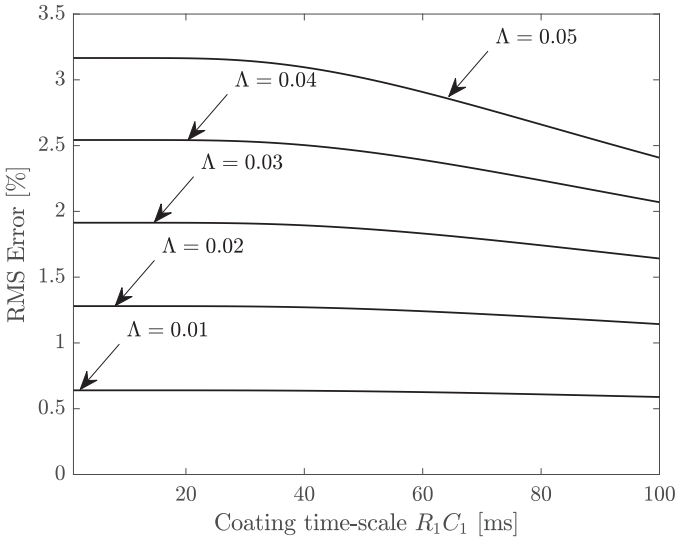

Fig. 4. Validation of two-layer approximate solution. RMS error as a function of coating time scale RC for different thermal inertia ratios Λ.

be observed for R_2C_2, but that is of less practical interest. For all cases, the error is below 3.5% when Λ is less than 0.05.

4. Superposition

As outlined above, the step-change solution can be used in conjunction with the principle of superposition in order to find the wall surface temperature given an arbitrary heat flux history. The surface temperature found using the full solution and low-Λ approximation are given, respectively, as

$$t_o(\theta_n) = \sum_{i=0}^{n} \left\{ \Delta\dot{q}_i'' \left[R_{total} - \sum_{m=1}^{\infty} \frac{B(s)|_{s=-\beta_m}}{\beta_m \frac{dD(s)}{ds}|_{s=-\beta_m}} e^{-\beta_m(\theta_n-\theta_i)} \right] \right\} \tag{28}$$

and

$$t_o(\theta_n) = \sum_{i=0}^{n} \left\{ \Delta\dot{q}_i'' \cdot \left[R_1 \left(1 - \frac{8}{\pi^2} \sum_{\nu=1}^{\infty} \frac{1}{(2\nu-1)^2} e^{-\frac{(2\nu-1)^2}{4R_1C_1}\pi^2(\theta_n-\theta_i)} \right) + R_2 \left(1 - \frac{8}{\pi^2} \sum_{\nu=1}^{\infty} \frac{1}{(2\nu-1)^2} e^{-\frac{(2\nu-1)^2}{4R_2C_2}\pi^2(\theta_n-\theta_i)} \right) \right] \right\} \tag{29}$$

where $\Delta\dot{q}_i'' = \left(\dot{q}_i'' - \dot{q}_{i-1}''\right)$. In both cases, the heat flux history is discretized and the incremental step change in heat flux is multiplied by a response factor (shown in the square brackets) and summed over all previous times. Particular attention should be paid to the time summation (index i). At time $\theta_0 = 0$, $\Delta q_0'' = -\bar{q}'' + \dot{q}_0''$ as discussed in Section 2.2.1. In the limit of long times in the past, the exponential terms go to zero and the response factor tends towards the total resistance, *i.e.* R_{total} in (28) and $R_1 + R_2$ in (29). This is related to the fact that after a certain amount of time has passed, the response to an earlier heat flux change has reached a steady state value.

Computationally, there are a few issues that one needs to address to maintain the desired efficiency. First, the number of roots to include in the solution needs to be limited to those that are necessary to ensure accuracy. For practical applications, the maximum root must be found to ensure a precision of ϵ for the smallest timestep so that: $e^{-\beta_{\max}\Delta\theta_{\min}} < \epsilon$. Second, the summation over time (index i) only needs to be performed until the response function has reached its steady state value; call this time θ_k where for

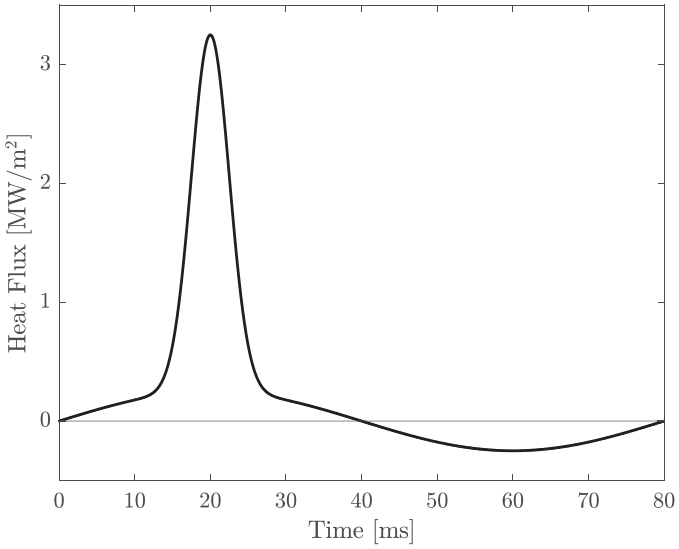

Fig. 5. Gaussian added to a sinusoidal surface heat flux input.

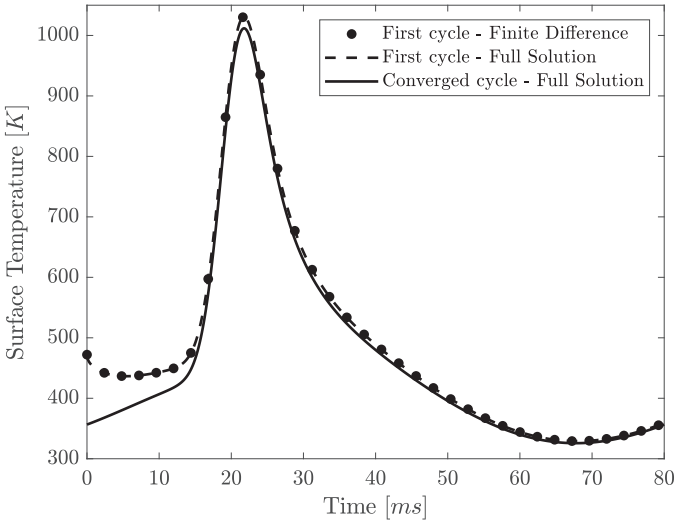

Fig. 6. Surface temperature as a function of time for a three-layer problem (for material properties, see text) subjected to a prescribed surface heat flux.

illustration purposes $\theta_k < \theta_n$. For times $\theta < \theta_k$ the result can just be found as the summation up to k of the heat flux changes, which is just the product of the total heat flux to the wall before θ_k and the total resistance. In practice, this can be kept as a running sum to reduce cost. Using Eq. (29) as a guide, one sees that the exponential term in the response is a function of $\frac{\theta}{R_i C_i}$, and therefore one expects the time for the response to stabilize to be proportional to $\max(R_i C_i)$, in practice a proportionality constant of 10 has been found to suffice. Finally, for large data sets it will be more efficient to split the response factor into two parts. The first part will be comprised of the R_{total} term, which is just multiplied by the sum of the heat flux steps. The second term is comprised of the sum of the terms including the exponential, which tend towards zero at long times. The latter expression can be most efficiently calculated using the convolution of the heat flux change with this modified response factor.

By way of example, a simulated in-cylinder heat flux was constructed as the sum of a sinusoidal function and a Gaussian. The positive portion of the sinusoid represents the compression and expansion, and the negative portion represents the heat flux reversal that occurs during the intake stroke. The Gaussian term simulates the effect of combustion, and the Gaussian was delayed so that it would peak at the same time as the positive sinusoid. Fig. 5 shows one cycle of the simulated heat flux for a case with a peak Gaussian heat flux of 3 MW/m^2, a sinusoid magnitude of 0.25 MW/m^2, an equivalent of 1500 rpm engine speed, and a Gaussian full-width at half-maximum value of 5.9 ms. A three-layer wall was considered. Layer 1 was a 100 μm TS coating, layer 2 was a YSZ coating of 150 μm, and layer 3, the remainder of the domain, was aluminum. The total domain length was 5mm. The surface temperature was calculated using both (28) and the finite difference code mentioned above.

The full and finite difference solution for the three-layer problem is shown in Fig. 6. Two different cycles are shown. The first cycle is shown in a dashed line with the symbols being the finite difference solution. Excellent agreement is seen between the two solutions. The first cycle is shown to highlight the treatment of the initial condition. The finite difference temperature domain was initialized using the steady solution derived from the cycle-mean heat flux, $\bar{q}''$ which is known in this case. The full inversion solution starts at time zero with a heat flux step of $-\bar{q}''$ as discussed in Section 2.2.1. It can be seen that virtually identical results are observed. The converged cycle shown in Fig. 6 is only shown for the full solution, but the agreement with the finite difference solution was excellent. Convergence was obtained in just a few cycles.

5. Discussion

The mathematical form of (29) suggests a way to non-dimensionalize the two-layer problem of interest subjected to periodic heat fluxes, similar to those found in internal combustion engines. The amplitude of the surface temperature swing over a cycle should be normalized by the maximum heat flux swing and total resistance, $R_{total} = R_1 + R_2$, to give a non-dimensional temperature swing, Θ, as

$$\Theta = \frac{t_{max} - t_{min}}{\left(\dot{q}''_{max} - \dot{q}''_{min}\right) R_{total}} \tag{30}$$

The maximum heat flux swing was chosen to bound the value to unity. There are three independent parameters that arise from (29): Ξ, Ω_1, and Ω_2, given by

$$\Xi \equiv \frac{R_1}{R_2} \tag{31}$$

$$\Omega_1 \equiv f R_1 C_1 \tag{32}$$

$$\Omega_2 \equiv f R_2 C_2 \tag{33}$$

where f is the frequency corresponding to the periodic excitation. It has been verified that over a wide range of R_i, C_i, and f, chosen in a way that Ξ, Ω_1, and Ω_2 are held constant, the dependent parameter Θ is also constant for both the full inversion and low-Λ solutions.

The utility of this approach will be demonstrated by assuming a sinusoidally varying heat flux imposed at x=0. The fact that there are three independent parameters makes visualization difficult. In practice, one wants to know the ability of the surface temperature to swing to follow the imposed heat flux as the frequency of oscillation and coating properties change. A series of two-layer simulations were performed using the full solution where Ξ and Ω_1 were varied while Ω_2 was held constant. This approach was taken to allow simple visualization of the results. The substrate material properties (R_2 and C_2) are normally fixed while the coating properties are adjusted in the design phase; note Ω_2 can still change via f.

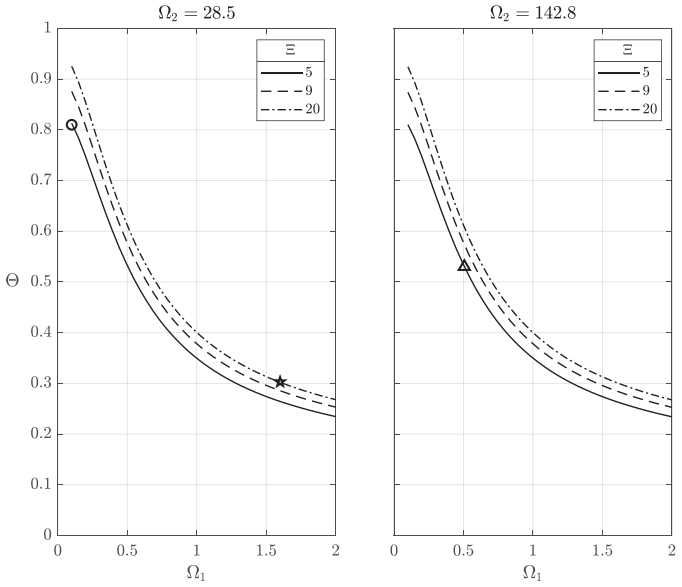

Fig. 7. Dimensionless response of two-layer wall subjected to a sinusoidal heat flux.

Fig. 7 shows results for Ω_2=28.5 (left) and Ω_2=142 (right). The first thing to notice is that the effect of Ω_2 is very small for the range of conditions tested. The conditions were chosen to be representative of internal combustion engines with thermal-swing coatings, *i.e.*, $R_1 > R_2$ and $R_1C_1 << R_2C_2$. Therefore, the effect of excitation frequency change can be, more or less, isolated to Ω_1. Either graph in Fig. 7 can then be taken to give the general solution to this problem.

Consider first the case of increasing the coating thickness by a factor of four with all other geometric and material properties held fixed. The response to this change is complicated. The value of Ξ increases by four; Ω_1 increases by a factor of 16; and Ω_2 remains constant. For the situation where the initial case has Ξ=5, Ω_1=0.1, and Ω_2=28.5, shown as the open circle in Fig. 7, the modified state has Ξ=20, Ω_1=1.6, and Ω_2=28.5, shown as the star in Fig. 7. For this change, Θ would decrease from 0.81 to 0.30. The actual temperature swing, however, would *increase* by about 50% due to the increase in R_1. The coating is less efficient, but gives the desired effect of higher temperature swings.

Another typical case is the response of a fixed system to changes in frequency of the input, which corresponds to a change in the engine speed. Starting from the same initial point as the previous example, an increase in speed by a factor of five would result in Ξ=5, Ω_1=0.5, and Ω_2=142, shown as the triangle in Fig. 7. In this scenario, Θ decreases from 0.81 to 0.53, which gives a corresponding *decrease* in temperature swing. This underscores that thermal-swing coatings reduce their effectiveness at higher frequency.

5.1. Advantages of presented method

Before discussing the advantages of the present method, it is useful to consider the alternative approach of using an implicit finite difference code; the Crank-Nicolson method was employed in the current work. An implicit solution guarantees stability for any time step size but does not guarantee convergence, *i.e.*, sufficient temporal resolution is required to avoid an oscillatory solution. The subsequent comparisons will be made for a two-layer problem for an operating condition very similar that of Fig. 6 and the assessment of absolute error is made by comparing the results to a very highly resolved finite difference solution.

The wall surface temperature can be computed in either an uncoupled or coupled manner. In the uncoupled manner, one knows the applied heat flux in terms of heat transfer coefficient and gas temperature for a given operating condition (or multiple), and wants to screen a large number of possible coatings or design an optimal coating that will minimize heat loss. In the coupled approach, the wall temperature solution is coupled to another combustion simulation code. At each time step of the combustion simulation, the wall temperature needs to be updated.

A 0.1K root mean square temperature error threshold was defined as acceptable. For the analytical method, the only source of error is in the discretization of the applied heat flux into a series of step changes, but for the finite difference solution there is also the spatial discretization error. In the uncoupled operation mode, the analytical approach required approximately 8000 time steps to complete one cycle at the desired accuracy, and computed in less than 1 ms using MATLAB on a Windows machine with a 3.00Ghz Intel Core i5 processor and 16GB of RAM. In contrast, the lowest spatial resolution finite difference case that met the error criteria took 25× longer on the same computer because it had to compute all of the node temperatures at each time step up to the final time (it did, however, require fewer times steps than the analytical case). Clearly, in the coating screening or design phase, the analytical approach provides substantial time savings.

For the coupled mode of operation, the situation is different. For the finite difference code the computational time is the same as above. The analytical solution, in contrast, needs to be calculated at each time step using the heat flux history up to that point in time, which slows down the speed. In practice, the coupled analytical solution was about 10× slower than the finite difference solution for the two-layer problem. In fact, when additional layers are added to the problem, the computational times remain constant only for the analytical solution. The finite difference requires further discretization therefore the computational time increases. There are a few steps that can be implemented to improve the speed of the analytical solution in the coupled situation. The analytical solution does not have a time step requirement, so for times during the cycle with slowly varying heat flux, the time step can be lengthened with little loss of accuracy. Additionally, one would probably not operate the finite difference solution with the minimum required spatial resolution to prevent potential issues from, for example, operating condition changes.

6. Conclusions

The problem of a plane, coated wall with a time-varying heat flux applied to one surface and the other held at a constant temperature was investigated analytically under the assumption of one-dimensional heat flow in a plane wall with constant thermophysical properties. The problem is linear, and superposition was used to determine the input surface temperature. The applied heat flux was discretized into a series of step changes, and surface temperature is found by combining the solution for a single step change of heat flux. Two solutions were obtained to the step-change problem, the full solution and one found under the additional assumption that the coating's thermal inertia $\sqrt{k\rho c}$ was much less than that of the substrate, which is valid for thermal-swing coatings. The solutions were obtained using the matrix method in conjunction with the 1-D Laplace transformed heat diffusion equation. The full solution method, which is extendable to any number of layers, relies on the numerical evaluation of roots to invert to the time domain. The low-Λ solution is fully analytical, but is limited to a single coating layer.

The low-Λ analytical solution served as the basis of a non-dimensionalization of the general problem of a two-layer wall subjected to a periodic heat flux. Three independent dimensionless

parameters were derived; for thermal-swing type coatings only two were relevant. The dependent parameter was the surface temperature swing, which was normalized by the total wall resistance and the maximum swing in the surface heat flux. The dimensionless system was demonstrated for a sinusoidal imposed heat flux, and several examples of its utility were provided.

Declaration of Competing Interest

The authors declare that they have no known competing financial interests or personal relationships that could have appeared to influence the work reported in this paper.

The authors declare the following financial interests/personal relationships which may be considered as potential competing interests:

CRediT authorship contribution statement

G. Koutsakis: Conceptualization, Methodology, Software, Formal analysis, Investigation, Resources, Data curation, Writing - original draft, Visualization. **G.F. Nellis:** Writing - review & editing. **J.B. Ghandhi:** Conceptualization, Writing - review & editing, Supervision, Project administration, Funding acquisition.

Acknowledgments

Support for this work was provided by John Deere & Company.

References

[1] J.B. Heywood, Internal Combustion Engine Fundamentals, McGraw-Hill, 1988.
[2] R. Kamo, Adiabatic turbocompound engine performance prediction, SAE Technical Papers (1978), doi:10.4271/780068.
[3] R. Kamo, W. Bryzik, Ceramics in heat engines, Passenger Car Meeting & Exposition, SAE International, 1979, doi:10.4271/790645.
[4] N.P. Padture, M. Gell, E.H. Jordan, Thermal barrier coatings for gas-turbine engine applications, Science 296 (5566) (2002) 280–284.
[5] T. Hendricks, J. Ghandhi, Estimation of surface heat flux in IC engines using temperature measurements: processing code effects, SAE Int. J. Engines 5 (3) (2012) 1268–1285.
[6] D.N. Assanis, K. Wiese, E. Schwarz, W. Bryzik, The effects of ceramic coatings on diesel engine performance and exhaust emissions, SAE Technical Paper Series, 1, 1991, doi:10.4271/910460.
[7] K. Osawa, R. Kamo, E. Valdmanis, v, SAE Technical Paper Series, 1, 1991, doi:10.4271/910461.
[8] S. Chan, K. Khor, The effect of thermal barrier coated piston crown on engine characteristics, J. Mater. Eng. Perform. 9 (1) (2000) 103–109, doi:10.1361/105994900770346358.
[9] K.Z. Mendera, Effectiveness of plasma sprayed coatings for engine combustion chamber, SAE Technical Paper Series 1 (724) (2000), doi:10.4271/2000-01-2982.
[10] P. Schihl, E. Schwarz, W. Bryzik, Performance characteristics of a low heat rejection direct-Injection military diesel engine retrofitted with thermal barrier coated pistons, J. Eng. Gas Turbine.Powe.r 123 (3) (2001) 644, doi:10.1115/1.1370372.
[11] R. Kamo, N.S. Mavinahally, L. Kamo, W. Bryzik, E.E. Schwartz, Injection Characteristics that Improve Performance of Ceramic Coated Diesel Engines, 1999. 10.4271/1999-01-0972
[12] D.W. Dickey, The effect of insulated combustion chamber surfaces on direct-injected diesel engine performance, emissions and combustion, SAE Technical Paper Series, 1, 1989, doi:10.4271/890292.
[13] W.K. Cheng, V.W. Wong, F. Gao, Heat, 1989, doi:10.4271/890570.
[14] J.A. Gatowski, Evaluation of a selectively-cooled single-cylinder 0.5-L diesel engine, SAE Trans. (1990) 1580–1591.
[15] G. Woschni, W. Spindler, K. Kolesa, Heat insulation of combustion chamber walls a measure to decrease the fuel consumption of I.C. engines? SAE Technical Papers, 1, 1987, doi:10.4271/870339.
[16] S. Furuhama, Y. Enomoto, Heat transfer into ceramic combustion wall of internal combustion engines, 1987. 10.4271/870153
[17] A.C. Alkidas, Performance and emissions achievements with an uncooled heavy-duty, single-cylinder diesel engine, 1989. 10.4271/890144
[18] J.C. Huang, G.L. Borman, Measurements of instantaneous heat flux to metal and ceramic surfaces in a diesel engine, 1, 1987, doi:10.4271/870155.
[19] H. Kosaka, Y. Wakisaka, Y. Nomura, Y. Hotta, M. Koike, K. Nakakita, A. Kawaguchi, Concept of “temperature swing heat insulation” in combustion chamber walls, and appropriate thermo-Physical properties for heat insulation coat, SAE Int. J. Engines 6 (1) (2013) 2013–01–0274, doi:10.4271/2013-01-0274.
[20] T. Horie, F. Shimizu, N. Nishikawa, Special feature: challenges of internal combustion engines for development of thermo-swing insulation coat cäSiPRA” 48 (4) (2017) 11–17.
[21] A. Kawaguchi, H. Iguma, H. Yamashita, N. Takada, N. Nishikawa, C. Yamashita, Y. Wakisaka, K. Fukui, Thermo-Swing wall insulation technology; - A novel heat loss reduction approach on engine combustion chamber, SAE Technical Paper Series 1 (2016), doi:10.4271/2016-01-2333.
[22] R.P. Durrett, P.M. Najt, P.P. Andruskiewicz IV, T.A. Schaedler, G.P. Hill, J.H. Martin, C.J. Ro, Internal combustion engine and method for coating internal combustion engine components, 2019. US Patent 10,190,533.
[23] M. Andrie, S. Kokjohn, S. Paliwal, L.S. Kamo, A. Kamo, D. Procknow, Low heat capacitance thermal barrier coatings for internal combustion engines, SAE Technical Paper Series 1 (2019) 1–13, doi:10.4271/2019-01-0228.
[24] G. Nellis, S. Klein, Heat transfer, Cambridge University Press, 2009.
[25] D.N. Assanis, J.B. Heywood, development and use of a computer simulation of the turbocompounded diesel system for engine performance and component heat transfer studies, 1986. 10.4271/860329
[26] V.W. Wong, W. Bauer, R. Kamo, W. Bryzik, M. Reid, Assessment of thin thermal barrier coatings for I.C. engines, SAE Technical Paper Series, 1, 1995, doi:10.4271/950980.
[27] S. Caputo, F. Millo, G. Cifali, F.C. Pesce, Numerical investigation on the effects of different thermal insulation strategies for a passenger car diesel engine, SAE Int. J. Eng. 10 (4) (2017) 2154–2165.
[28] M. Yao, T. Ma, H. Wang, Z. Zheng, H. Liu, Y. Zhang, A theoretical study on the effects of thermal barrier coating on diesel engine combustion and emission characteristics, Energy 162 (2018) 744–752, doi:10.1016/j.energy.2018.08.009.
[29] A. Poubeau, A. Vauvy, F. Duffour, J.-M. Zaccardi, G. de Paola, M. Abramczuk, Modeling investigation of thermal insulation approaches for low heat rejection diesel engines using a conjugate heat transfer model, Int. J. Engine Res. 20 (1) (2018) 92–104, doi:10.1177/1468087418818264.
[30] N. Killingsworth, T. Powell, R. O’Donnell, Z. Filipi, M. Hoffman, Modeling the effect of thermal barrier coatings on HCCI engine combustion using CFD simulations with Conjugate Heat Transfer, Technical Report, 2019.
[31] G. Borman, K. Nishiwaki, Internal-combustion engine heat transfer, Prog. Energy Combust. Sci. 13 (1) (1987) 1–46, doi:10.1016/0360-1285(87)90005-0.
[32] L.A. Pipes, Matrix analysis of heat transfer problems, J. Franklin Inst. 263 (3) (1957) 195–206.
[33] H. Carslaw, J. Jaeger, Conduction of heat in solids, 1959. 10.1371/journal.pone.0041178
[34] R.V. Churchill, J.W. Brown, Complex Variables and Applications, 8th edition, 2009.